Rapid Communications Featured in Physics

Characterization of two- and one-dimensional water networks on Ni(111) via atomic force microscopy

Akitoshi Shiotari * and Yoshiaki Sugimoto
Department of Advanced Materials Science, The University of Tokyo, Kashiwa 277-8561, Japan

Hiroshi Kamio
Nippon Steel Corporation, 293-8511 Futtsu, Japan

(Received 30 June 2019; published 19 September 2019)

Determination of the adsorption structure of water molecules on metal surfaces is an imperative challenge to understanding the mechanisms of the wetting process and water-related heterogeneous catalysis. We identify water monolayers formed on Ni(111) via low-temperature atomic force microscopy, which enables the visualization of individual water molecules in monolayers with higher spatial resolution than scanning tunneling microscopy. On the terraces of Ni(111) at 150 K, water forms monolayers comprising fused pentagonal, hexagonal, and heptagonal rings. Water adsorbates on step sites assemble in a different manner, forming a hydrogen-bonding network with fused pentagonal and octagonal rings aligned in the step direction. Because similar water networks with pentagonal rings have been proposed in monolayers or their defect sites on other metal surfaces, our structural characterization of $H_2O/Ni(111)$ provides an insight into water adsorption structures on metals.

DOI: 10.1103/PhysRevMaterials.3.093001

I. INTRODUCTION

Nickel (Ni) is a versatile metallic component of alloys and cell electrodes. Adsorption of H_2O molecules on Ni-based materials is closely associated with various surface chemical and physical phenomena, such as wetting, corrosion, and electrochemical reactions. In addition, Ni surfaces can provoke heterogeneous catalyses such as the water–gas shift reaction [1] and steam reforming [2]. Therefore, adsorption and dissociation of water molecules on Ni(111), in particular, have been studied both experimentally [3–11] and theoretically [10–18] to understand their catalytic mechanisms. Theoretical comparisons among several metal surfaces have predicted that water tends to (partially) dissociate on Ni(111), in contrast to Pd(111) and Pt(111) [19–21]. However, heating $H_2O/Ni(111)$ induces water to desorb from the surface instead of dissociating [8,9,18]. This reaffirms that accurate determination of adsorption structures is indispensable for investigating the reactivity and dynamics of water at Ni(111).

On metal surfaces, water molecules assemble via hydrogen (H) bonding to yield various types of clusters and monolayers [22–25], complicating the characterization of the adsorption structures. For $H_2O/Ni(111)$ at submonolayer regimes, Gallagher *et al.* [7] revealed a $(\sqrt{28} \times \sqrt{28})R19^\circ$ pattern with low-energy electron diffraction. Subsequently, the density functional theory (DFT) calculations by Thürmer *et al.* [11] helped establish a model of a structure wherein water molecules are H bonded to form pentagonal, hexagonal, and heptagonal rings, in a manner analogous to the proposed structure for $(\sqrt{37} \times \sqrt{37})R25^\circ$-$H_2O/Pt(111)$ [26]. However, this ordered monolayer has not been corroborated via direct observation methods such as scanning tunneling microscopy (STM) [11]. In addition to adsorbates on terraces, the adsorption structures on step sites deserve attention because step edges strongly contribute to the diffusivity, layer growth, and catalytic reactions of water adsorbates [27–32]. Although water molecules on stepped Ni surfaces have been predominantly investigated via theoretical calculations [33–37], few experimental studies have explored local adsorption structures [38].

Herein, we observe $H_2O/Ni(111)$ using low-temperature STM and atomic force microscopy (AFM). AFM with a tip terminated by a single atom/molecule can not only visualize the intramolecular structures of organic molecules [39–41] but also the individual H_2O molecules in H-bonding assemblies [42–45]. Through AFM imaging with higher spatial resolution than STM, we establish structural models of two- and one-dimensional (2D and 1D) water networks that are formed on the terraces and at step edges, respectively.

II. METHODS

The experiments were conducted in an ultrahigh-vacuum chamber (Omicron low-temperature STM/AFM system) at 4.8 or 78 K. A tuning fork with an etched tungsten tip was used as a force sensor in the frequency-modulation mode [41] (resonance frequency of 21.3 kHz, spring constant of $\sim$1800 N/m, quality factor of 4–5 $\times 10^4$, and oscillation amplitude of 100 pm). Single-crystalline Ni(111) was cleaned by repeated cycles of Ar^+ sputtering and annealing. Ultra-pure water (Wako Pure Chemical Industries, Ltd.) was purified via freeze-and-pump cycles. The surface at $\sim$6 K was exposed to CO gas (as required) to fabricate a CO tip [46]. AFM images were acquired in constant-height mode at a sample bias of $V = 0$ mV with a CO tip whereas STM images were

*shiotari@k.u-tokyo.ac.jp

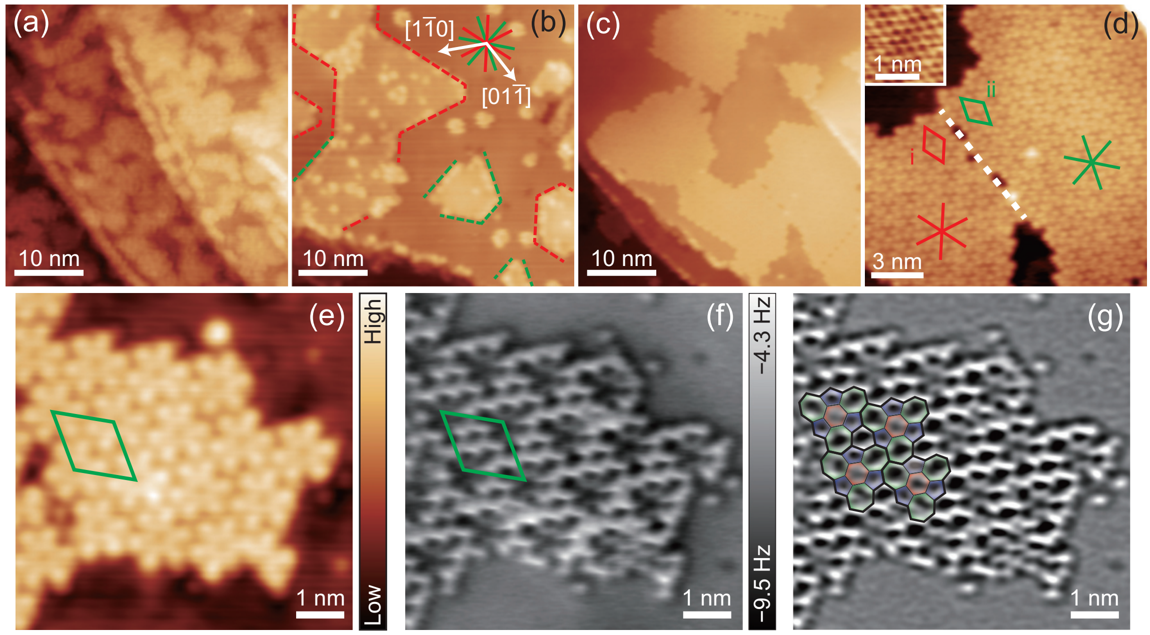

FIG. 1. (a) STM image of H_2O/Ni(111) at 78 K. (b),(c) STM image of the same sample as in (a) but after annealing at 145 and 150 K for 5 min, respectively. The red and green lines indicate the orientations of $\pm19^\circ$ relative to the Ni atomic lattice (white allows). (d) Magnified STM image of (c). Images in (a)–(d) were obtained with a metal tip [(a),(b) $V = -500$ mV, $I = 20$ pA, 78 K and (c),(d) $V = -200$ mV, $I = 20$ pA, 4.8 K]. The inset shows an atomically resolved STM image of the bare Ni surface obtained with a CO tip ($V = 10$ mV, $I = 2$ nA, 4.8 K). The red and green rhombuses represent the unit cells for domains i and ii of the $(\sqrt{28} \times \sqrt{28})R19^\circ$ superstructure, respectively. (e),(f) STM ($V = 30$ mV, $I = 20$ pA) and AFM ($z = -135$ pm) images of an island of domain ii, respectively, obtained with a CO tip at 4.8 K. (g) Laplacian-filtered image in (f). The blue, red, and green flames indicate the pentagonal, hexagonal, and heptagonal rings, respectively.

obtained in the constant-current mode. The origin of the tip height z is the set-point height determined via STM over the bare Ni surface at $V = 30$ mV and tunneling current $I = 20$ pA. Here, $z < 0$ implies that the tip is closer to the sample than the origin. Force curves $F(z)$ were calculated using the Sader formula [47] from the frequency shift curves $\Delta f(z)$ recorded at $V = 0$ mV.

III. RESULTS AND DISCUSSION

Figure 1(a) shows an STM image of Ni(111) exposed to H_2O gas at 78 K. Water forms islands covering about 70% of the surface [$\sim$0.7 monolayers (ML)]. No ordered patterns were observed on the islands, implying that water molecules are arranged amorphously. By annealing the sample at 145 K, the coverage was decreased to $\sim$0.4 ML through molecular desorption. Then, small clusters of diameters $\sim$1 nm were predominantly observed together with large islands [Fig. 1(b)], in good agreement with the results of a previous STM study of $\sim$0.5 ML H_2O/Ni(111) [11]. Additionally, we confirmed that similar structures were observed on Ni(111) exposed to H_2O at 140 K. As indicated by red and green lines in Fig. 1(b), the outlines of the islands are mainly constructed by triangles with most edges oriented by $\pm19^\circ$ relative to the unit vectors of the Ni(111) atomic lattice [white arrows; see also the inset of Fig. 1(d) showing an atom-resolved STM image of the bare Ni surface]. Therefore, we ascribe the large islands to a transitive structure leading to the well-ordered $(\sqrt{28} \times \sqrt{28})R19^\circ$ superstructure. Furthermore, through high-resolution AFM, we revealed that the small cluster includes a central hexagonal ring of $(H_2O)_6$ (see the Supplemental Material [48]), which probably nucleates the initial growth of H-bonding water networks on the surface [6].

Upon further annealing the sample at 150 K, the small clusters disappeared, and homogeneous huge islands became dominant on the surface [Fig. 1(c)]. As shown in Fig. 1(d), the island has an ordered pattern with a periodicity of 13 nm, and the unit cell is oriented by $+19^\circ$ or -19° relative to the Ni atomic lattice. Two domains with different orientations [labeled i and ii in Fig. 1(d)] coexisted on the surface and were separated by boundaries on the island (white dotted line). Thus, the water layer is assigned to a $(\sqrt{28} \times \sqrt{28})R19^\circ$ superstructure [7]. A magnified STM image reveals that the island is composed of hexagonally arranged hexapetal protrusions [Fig. 1(e)]. Figures 1(f) and 1(g) show AFM and Laplacian-filtered AFM images of the island, respectively, where bright spots reflect the lateral positions of the O atoms of water molecules [42]. This indicates that the hexapetal unit contains a central hexagonal ring [red flames in Fig. 1(g)] surrounded by alternately fused three pentagonal (blue flames) and heptagonal (green flames) rings each. This appearance suggests that water molecules in the island are seamlessly H bonded to each other.

For the $(\sqrt{28} \times \sqrt{28})R19^\circ$-$H_2O$/Ni(111), the H-bonding network with pentagonal and heptagonal rings was presumed by Thürmer *et al.* [11]. They termed it the "$\sqrt{28}$ di-vacancy structure" [Fig. 2(f)], and it is similar to the AFM pattern shown in Fig. 1(f). To obtain further information about this island, we investigated the z dependence of AFM images [Figs. 2(b)–2(e)] for the same area as that observed in an STM

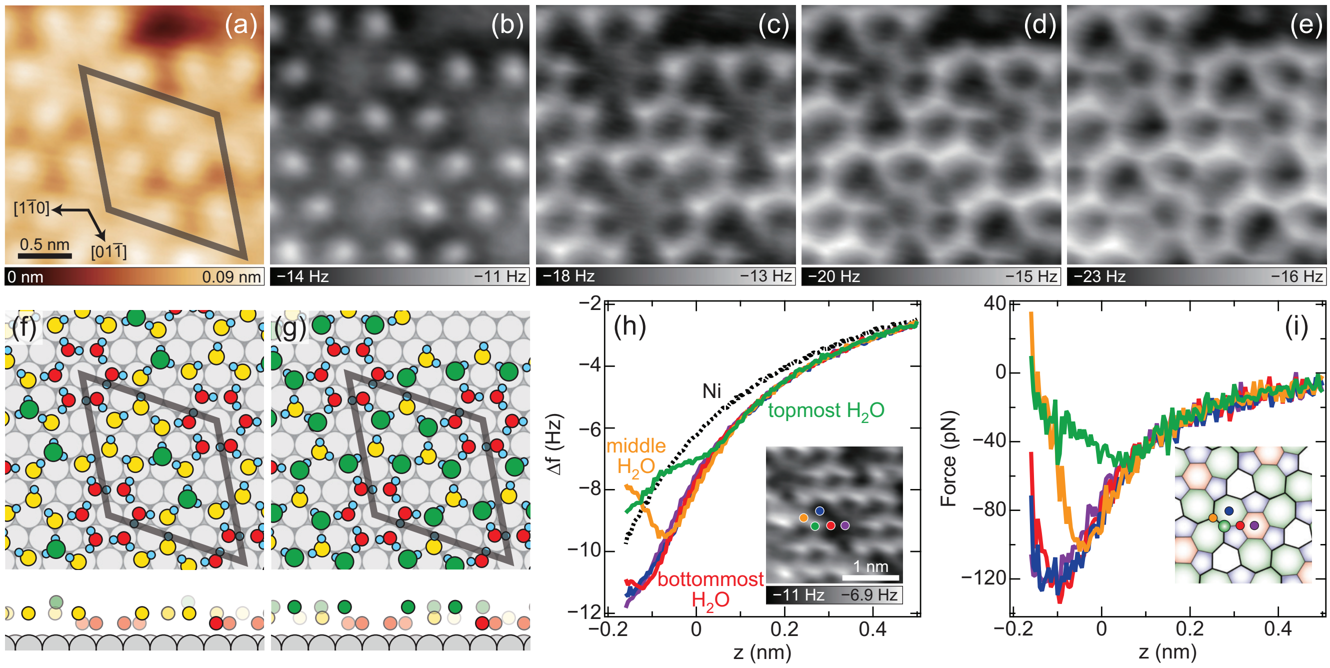

FIG. 2. (a) STM image of an island of domain ii ($V = 30$ mV, $I = 20$ pA, 4.8 K, CO tip). (b)–(e) AFM images of the same area as in (a) with $z = -50$, -100, -150, and -200 pm, respectively. (f) Schematic of the DFT-optimized "$\sqrt{28}$ di-vacancy structure" reported in Ref. [11]. The gray, cyan, red, yellow, and green spheres represent Ni, H, bottommost O, middle O, and topmost O atoms, respectively. The gray rhombus represents the unit cell of $(\sqrt{28} \times \sqrt{28})R19^\circ$. (g) Schematic structure of the water monolayer proposed according to the AFM appearances. The bottom panels of (f) and (g) show side-view illustrations of the structures (H atoms are not shown for clarity). The vertical distance between the bottommost H_2O and the substrate in (g) is tentatively assumed to be the same as that in (f). (h) $\Delta f(z)$ curves recorded over the markers in the inset (4.8 K, CO tip). The inset shows an AFM image of domain i ($z = -110$ pm). (i) Short-range force curves calculated from (h) after subtraction of the contribution of the bare Ni surface [black curve in (h)]. The inset schematically shows the water network for the inset image in (h).

image of the island [Fig. 2(a)]. At large z, the molecule located at each petal lobe in the STM image is visible through AFM [Fig. 2(b)], suggesting that this molecule highly protrudes toward vacuum [namely, topmost H_2O; green spheres in Fig. 2(g)]. For small z [Fig. 2(c)], other water molecules were visualized [yellow spheres in Fig. 2(g); middle H_2O]. The six water molecules located near the center of the hexapetal pattern [red spheres in Fig. 2(g); bottommost H_2O] eventually became visible when the tip moved closer to the sample [Figs. 2(d) and 2(e)]. Thus, the O atoms of water molecules in the island are of three types depending on their vertical heights, corresponding to the six topmost, four middle, and six bottommost H_2O molecules in each unit cell. The water molecules are consistently H bonded; for example, the neighbors of a bottommost H_2O molecule are two other bottommost molecules and a topmost H_2O, whereas a middle H_2O molecule is always surrounded by three topmost H_2O molecules [Fig. 2(g)]. Although the lateral positions of the O atoms in the AFM images are quite similar to that of the DFT-calculated "$\sqrt{28}$ di-vacancy structure" [11], their vertical positions are different [two topmost, eight middle, and six bottommost H_2O molecules in each unit cell for the "$\sqrt{28}$ di-vacancy structure;" see side-view illustrations in Figs. 2(f) and 2(g)]. Note that the arrangement of H atoms shown in Fig. 2(g) is tentative; H atoms of water on metal surfaces are not directly observed in the AFM images [42], and H-atom locations should be clarified through theoretical calculations.

The existence of three types of O atoms was confirmed by measuring force curves. The green, yellow, and red curves in Fig. 2(h) show $\Delta f(z)$ recorded over the topmost, middle, and bottommost H_2O molecules, respectively, in an island shown by the inset AFM image in Fig. 2(h). The short-range force curves were derived [Fig. 2(i)] by subtracting the background contribution of the bare Ni surface [Fig. 2(h), black]. At large z, attractive forces are almost equally applied over any location on the island probably because of the dense molecular network. At a close tip distance, the repulsive force applied on the water adsorbates was stronger than that applied over the hollows of the hexagonal [Fig. 2(i), purple] and heptagonal [Fig. 2(i), blue] rings, generating the molecule-resolved AFM image [Figs. 2(c)–2(e)]. The minimum force was detected at $z \approx +50$, -50, and -100 pm for the topmost, middle, and bottommost H_2O, respectively; this variation of the minimum force mainly originates from the vertical height difference among the O atoms [schematically shown in the bottom panel of Fig. 2(g)]. However, the molecular height would be modified by the AFM measurement. The slope in the repulsive region ($z < 50$ pm) for the topmost H_2O is very moderate ($\sim$0.4 Nm^{-1}), which differs from the slopes of the other H_2O on the surface and H_2O/Cu(110) [42] ($\sim$0.8–1 Nm^{-1}). This implies that the topmost H_2O is readily displaced against the

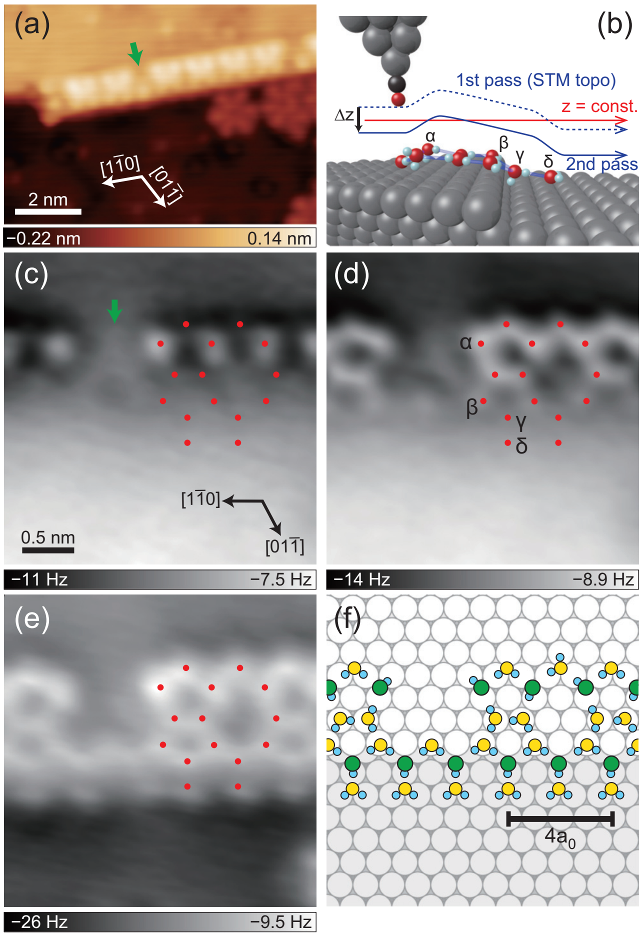

FIG. 3. (a) STM image of a monoatomic step of H_2O/Ni(111) ($V = 30$ mV, $I = 20$ pA, 4.8 K, CO tip). The green arrow indicates a characteristic defect in the water networks at the step edge. (b) Schematic structure of the step and the tip. The gray, cyan, red, and black spheres represent Ni, H, O, and C atoms, respectively. The scanning trajectory for AFM imaging are also shown schematically. (c),(d) Constant-height AFM images of the step edge in (a), obtained with $z = -60$ and -135 pm, respectively. (e) AFM image of the same area as in (c) and (d) but with the tip trajectory aligned to the STM topography as shown by the blue solid curve in (b) ($V = 30$ mV and $I = 20$ pA for STM; $V = 0$ mV and $\Delta z = -210$ pm for AFM). The red dots represent the O-atom positions based on (e). (f) Schematic structure of the water network at the step edge proposed according to the AFM appearances.

tip because this molecule is located far from surface Ni atoms. The relaxation of the repulsive force provides the contrast inversion between the topmost and middle molecules in the AFM images [Figs. 2(c)–2(e)].

While the islands of $(\sqrt{28} \times \sqrt{28})R19^\circ$ dominate on terraces, water molecules form a different ordered structure on the step sites of the surface. Figure 3(a) shows an STM image of a monoatomic step. At the edge of the upper terrace, H-shaped protrusions are aligned in the step direction (i.e., the [1$\bar{1}$0] direction) with a periodicity of 1.0 nm, which equals four times the Ni atomic distance a_0 (0.249 nm). The periodic structure has some defects, one of which is imaged as a single protrusion indicated by the green arrow in Fig. 3(a). We obtained constant-height AFM images of the edge structure, including the defect [Figs. 3(c) and 3(d)]. At large z [Fig. 3(c)], only one type of adsorbate [labeled as α in Figs. 3(b) and 3(d)] appears as a protrusion, which is assigned to the topmost H_2O on the upper terrace. When the tip is closer [Fig. 3(d)], other molecules on the upper terrace become visible. We tentatively assign the higher (lower) molecules to H_2O to a vertical (horizontal) molecular plane. According to the image [Fig. 3(d)], among the molecules on the upper terrace, the β-labeled H_2O is the closest to the edge.

Adsorbates on the lower terrace are too far from the tip to be visualized by constant-height imaging [red arrow in Fig. 3(b)]. Hence, we imaged the step-edge structure through multipass methods [49–51] as follows. First, we obtained a constant-current STM image and recorded the tip trajectory $z_{1st}(x, y)$ during the scan [first pass; Fig. 3(b), dotted blue arrow]. Next, the identical area was scanned again with a tip height determined by $z_{2nd}(x, y) = z_{1st}(x, y) + \Delta z$ to obtain a $\Delta f(x, y)$ map (second pass). During the second-pass scanning with negative Δz, the tip over the lower terrace was closer than that in the constant-height mode [Fig. 3(b), solid blue arrow]. Figure 3(e) shows the second-pass map, reflecting the positions of all H_2O molecules on the lower [labeled as γ and δ in Figs. 3(b) and 3(d)] and upper terraces. Although the first-pass STM image shows blurry H-shaped protrusions similar to those shown in Fig. 3(a), the second-pass map shows sharp features with a pattern different from the STM image, and the bright spots in the map originate from the repulsive atomic force between H_2O and the tip apex. As shown in Fig. 3(f), the unit cell of the ordered structure contains two pentagonal rings and an octagonal ring fused together with $4a_0$ periodicity, whereas the defect has no rings. The formation of such a 1D network has not been predicted in previous studies on water at stepped Ni surfaces [33–38], highlighting the importance of directly observing water assemblies on surfaces. This periodic structure is very similar to domain boundaries of H_2O/Ru(0001) [52], water islands on a stepped Cu(551) surface [32], and defect rows in the second water layer on SnPt(111) [53], suggesting that such a pentagonal-octagonal network is a typical defect in thin water layers on metal surfaces.

IV. CONCLUSIONS

In summary, we observed H_2O clusters and monolayers on Ni(111) via STM and AFM. Water molecules exist as disordered assemblies on the metal surface at 78 K, whereas they are rearranged at 140–145 K to yield small clusters with a central cyclic $(H_2O)_6$ core. Observation of the sample annealed at 150 K showed islands of the $(\sqrt{28} \times \sqrt{28})R19^\circ$ superstructure dominant on the terraces. High-resolution AFM imaging revealed that in the island, water molecules formed H-bonding networks, including pentagonal, hexagonal, and heptagonal rings. The molecular arrangement is consistent with the "$\sqrt{28}$ di-vacancy" model [11], despite the serious disagreement on the vertical height of each molecule. At a monoatomic step edge, H_2O forms another H-bonding network that contains pentagonal and octagonal rings with a periodicity of $4a_0$. Our determination of the ordered water networks on Ni(111) will be helpful in understanding the effect of intermolecular interactions on wettability in comparison to their behavior on other metal surfaces and in revealing the catalytic reactivity on both terraces and at step edges.

Notably, the H-bonding network of the $(\sqrt{28} \times \sqrt{28})R19^\circ$-$H_2O$/Ni(111) is quite similar to the proposed structure of the $(\sqrt{37} \times \sqrt{37})R25^\circ$-$H_2O$/Pt(111) [26]. However, the STM appearance of the water monolayer on Pt(111) (honeycomblike mesh with triangular depressions [26]) is distinctly different from that on Ni(111) [hexapetal-shaped protrusions; see Fig. 1(e)]. This strongly suggests that the structure of H_2O/Pt(111) can be researched further. Direct observation using high-resolution AFM must be a powerful approach toward the complete identification of the $\sqrt{37}$ structure and other water networks on various metal surfaces.

ACKNOWLEDGMENTS

This work was supported by JSPS KAKENHI Grants No. JP17K19024, No. JP18H01807, No. JP18H03859, and No. JP18K18990. A.S. acknowledges the support of ATI Research Grants 2017. Y.S. acknowledges the support of the Hattori Hokokai Foundation, Toray Science Foundation, and the Asahi Glass Foundation.

[1] K.-R. Hwang, C.-B. Lee, and J.-S. Park, Advanced nickel metal catalyst for water–gas shift reaction, J. Pow. Sour. **196**, 1349 (2011).

[2] J. Sehested, Four challenges for nickel steam-reforming catalysts, Catal. Today **111**, 103 (2006).

[3] T. E. Madey and F. P. Netzer, The adsorption of H_2O on Ni(111); influence of preadsorbed oxygen on azimuthal ordering, Surf. Sci. **117**, 549 (1982).

[4] R. Stulen and P. Thiel, Electron-stimulated desorption and thermal desorption spectrometry of H_2O on nickel (111), Surf. Sci. **157**, 99 (1985).

[5] T. Pache, H.-P. Steinrück, W. Huber, and D. Menzel, The adsorption of H_2O on clean and oxygen precovered Ni(111) studied by ARUPS and TPD, Surf. Sci. **224**, 195 (1989).

[6] M. Nakamura and M. Ito, Ring hexamer like cluster molecules of water formed on a Ni(111) surface, Chem. Phys. Lett. **384**, 256 (2004).

[7] M. Gallagher, S. Haq, A. Omer, and A. Hodgson, Water monolayer and multilayer adsorption on Ni(111), Surf. Sci. **601**, 268 (2007).

[8] J. Shan, J. F. Aarts, A. W. Kleyn, and L. B. Juurlink, The interaction of water with Ni(111) and H/Ni(111) studied by TPD and HREELS, Phys. Chem. Chem. Phys. **10**, 2227 (2008).

[9] W. Zhao, S. J. Carey, Z. Mao, and C. T. Campbell, Adsorbed hydroxyl and water on Ni(111): Heats of formation by calorimetry, ACS Catal. **8**, 1485 (2018).

[10] P. M. Hundt, B. Jiang, M. E. van Reijzen, H. Guo, and R. D. Beck, Vibrationally promoted dissociation of water on Ni(111), Science **344**, 504 (2014).

[11] K. Thürmer, S. Nie, P. J. Feibelman, and N. C. Bartelt, Clusters, molecular layers, and 3D crystals of water on Ni(111), J. Chem. Phys. **141**, 18C520 (2014).

[12] M. Pozzo, G. Carlini, R. Rosei, and D. Alfè, Comparative study of water dissociation on Rh(111) and Ni(111) studied with first principles calculations, J. Chem. Phys. **126**, 164706 (2007).

[13] J. Li, S. Zhu, Y. Li, E. E. Oguzie, and F. Wang, Electronic structure of monomeric water adsorption on Ni{111}: Beyond the general model, J. Phys. Chem. C **112**, 8301 (2008).

[14] W. Wang and G. Wang, A theoretical study of water adsorption and dissociation on Ni(111) surface during oxidative steam reforming and water gas shift processes, J. Energy Inst. **88**, 112 (2015).

[15] B. Jiang and H. Guo, Dynamics of Water Dissociative Chemisorption on Ni(111): Effects of Impact Sites and Incident Angles, Phys. Rev. Lett. **114**, 166101 (2015).

[16] A. Mohsenzadeh, K. Bolton, and T. Richards, DFT study of the adsorption and dissociation of water on Ni(111), Ni(110) and Ni(100) surfaces, Surf. Sci. **627**, 1 (2014).

[17] Z.-Y. Du, Y.-X. Ran, Y.-P. Guo, J. Feng, and W.-Y. Li, A theoretical study on the role of water and its derivatives in acetic acid steam reforming on Ni(111), Appl. Surf. Sci. **419**, 114 (2017).

[18] L. Zhu, C. Liu, X. Wen, Y.-W. Li, and H. Jiao, Molecular or dissociative adsorption of water on clean and oxygen pre-covered Ni(111) surfaces, Cat. Sci. Technol. **9**, 199 (2019).

[19] A. Michaelides, A. Alavi, and D. A. King, Insight into H_2O-ice adsorption and dissociation on metal surfaces from first-principles simulations, Phys. Rev. B **69**, 113404 (2004).

[20] G.-C. Wang, S.-X. Tao, and X.-H. Bu, A systematic theoretical study of water dissociation on clean and oxygen-preadsorbed transition metals, J. Catal. **244**, 10 (2006).

[21] A. A. Phatak, W. N. Delgass, F. H. Ribeiro, and W. F. Schneider, Density functional theory comparison of water dissociation steps on Cu, Au, Ni, Pd, and Pt, J. Phys. Chem. C **113**, 7269 (2009).

[22] A. Hodgson and S. Haq, Water adsorption and the wetting of metal surfaces, Surf. Sci. Rep. **64**, 381 (2009).

[23] J. Carrasco, A. Hodgson, and A. Michaelides, A molecular perspective of water at metal interfaces, Nat. Mater. **11**, 667 (2012).

[24] S. Maier and M. Salmeron, How does water wet a surface? Acc. Chem. Res. **48**, 2783 (2015).

[25] T. K. Shimizu, S. Maier, A. Verdaguer, J.-J. Velasco-Velez, and M. Salmeron, Water at surfaces and interfaces: From molecules to ice and bulk liquid, Prog. Surf. Sci. **93**, 87 (2018).

[26] S. Nie, P. J. Feibelman, N. C. Bartelt, and K. Thürmer, Pentagons and Heptagons in the First Water Layer on Pt(111), Phys. Rev. Lett. **105**, 026102 (2010).

[27] M. Morgenstern, T. Michely, and G. Comsa, Anisotropy in the Adsorption of H_2O at Low Coordination Sites on Pt(111), Phys. Rev. Lett. **77**, 703 (1996).

[28] A. Picolin, C. Busse, A. Redinger, M. Morgenstern, and T. Michely, Desorption of H_2O from flat and stepped Pt(111), J. Phys. Chem. C **113**, 691 (2008).

[29] W. Wang, H. Zhang, W. Wang, A. Zhao, B. Wang, and J. Hou, Observation of water dissociation on nanometer-sized FeO islands grown on Pt(111), Chem. Phys. Lett. **500**, 76 (2010).
[30] H. H. Kristoffersen, J. Ø. Hansen, U. Martinez, Y. Y. Wei, J. Matthiesen, R. Streber, R. Bechstein, E. Lægsgaard, F. Besenbacher, B. Hammer, and S. Wendt, Role of Steps in the Dissociative Adsorption of Water on Rutile TiO_2(110), Phys. Rev. Lett. **110**, 146101 (2013).
[31] M. J. Kolb, R. G. Farber, J. Derouin, C. Badan, F. Calle-Vallejo, L. B. F. Juurlink, D. R. Killelea, and M. T. M. Koper, Double-Stranded Water on Stepped Platinum Surfaces, Phys. Rev. Lett. **116**, 136101 (2016).
[32] C. Lin, N. Avidor, G. Corem, O. Godsi, G. Alexandrowicz, G. R. Darling, and A. Hodgson, Two-Dimensional Wetting of a Stepped Copper Surface, Phys. Rev. Lett. **120**, 076101 (2018).
[33] D. Sebastiani and L. Delle Site, Adsorption of water molecules on flat and stepped nickel surfaces from first principles, J. Chem. Theory Comput. **1**, 78 (2005).
[34] T. Murakhtina, L. Delle Site, and D. Sebastiani, Vibrational frequencies of water adsorbed on (111) and (221) nickel surfaces from first principle calculations, ChemPhysChem **7**, 1215 (2006).
[35] D. W. Blaylock, Y.-A. Zhu, and W. H. Green, Computational investigation of the thermochemistry and kinetics of steam methane reforming over a multi-faceted nickel catalyst, Top. Catal. **54**, 828 (2011).
[36] R. C. Catapan, A. A. Oliveira, Y. Chen, and D. G. Vlachos, DFT study of the water–gas shift reaction and coke formation on Ni(111) and Ni(211) surfaces, J. Phys. Chem. C **116**, 20281 (2012).
[37] Y. Huang, C. Ling, M. Jin, J. Du, T. Zhou, and S. Wang, Water adsorption and dissociation on Ni surface: Effects of steps, dopants, coverage and self-aggregation, Phys. Chem. Chem. Phys. **15**, 17804 (2013).
[38] C. Benndorf and C. Mundt, H_2O adsorption on Ni(s)(111) surfaces: Evidence for a step induced influence on the adsorption geometry, J. Vac. Sci. Technol. A **10**, 3026 (1992).
[39] N. Pavliček and L. Gross, Generation, manipulation and characterization of molecules by atomic force microscopy, Nat. Rev. Chem. **1**, 0005 (2017).
[40] P. Jelínek, High resolution SPM imaging of organic molecules with functionalized tips, J. Phys.: Condens. Matter **29**, 343002 (2017).
[41] F. J. Giessibl, The qPlus sensor, a powerful core for the atomic force microscope, Rev. Sci. Instrum. **90**, 011101 (2019).
[42] A. Shiotari and Y. Sugimoto, Ultrahigh-resolution imaging of water networks by atomic force microscopy, Nat. Commun. **8**, 14313 (2017).
[43] H. Koshida, S. Hatta, H. Okuyama, A. Shiotari, Y. Sugimoto, and T. Aruga, Water–NO complex formation and chain growth on Cu(111), J. Phys. Chem. C **122**, 8894 (2018).
[44] J. Peng, J. Guo, P. Hapala, D. Cao, R. Ma, B. Cheng, L. Xu, M. Ondráček, P. Jelínek, E. Wang, and Y. Jiang, Weakly perturbative imaging of interfacial water with submolecular resolution by atomic force microscopy, Nat. Commun. **9**, 122 (2018).
[45] J. Peng, D. Cao, Z. He, J. Guo, P. Hapala, R. Ma, B. Cheng, J. Chen, W. J. Xie, X.-Z. Li, P. Jelínek, L.-M. Xu, Y. Q. Gao, E.-G. Wang, and Y. Jiang, The effect of hydration number on the interfacial transport of sodium ions, Nature (London) **557**, 701 (2018).
[46] L. Gross, F. Mohn, N. Moll, P. Liljeroth, and G. Meyer, The chemical structure of a molecule resolved by atomic force microscopy, Science **325**, 1110 (2009).
[47] J. E. Sader and S. P. Jarvis, Accurate formulas for interaction force and energy in frequency modulation force spectroscopy, Appl. Phys. Lett. **84**, 1801 (2004).
[48] See Supplemental Material at http://link.aps.org/supplemental/10.1103/PhysRevMaterials.3.093001 for details of high-resolution imaging of small clusters on Ni(111).
[49] C. Moreno, O. Stetsovych, T. K. Shimizu, and O. Custance, Imaging three-dimensional surface objects with submolecular resolution by atomic force microscopy, Nano Lett. **15**, 2257 (2015).
[50] S. Freund, A. Hinaut, N. Marinakis, E. C. Constable, E. Meyer, C. E. Housecroft, and T. Glatzel, Anchoring of a dye precursor on NiO(001) studied by non-contact atomic force microscopy, Beilstein J. Nanotechnol. **9**, 242 (2018).
[51] D. Martin-Jimenez, S. Ahles, D. Mollenhauer, H. A. Wegner, A. Schirmeisen, and D. Ebeling, Bond-Level Imaging of the 3D Conformation of Adsorbed Organic Molecules using Atomic Force Microscopy with Simultaneous Tunneling Feedback, Phys. Rev. Lett. **122**, 196101 (2019).
[52] S. Maier, B. A. J. Lechner, G. A. Somorjai, and M. Salmeron, Growth and structure of the first layers of ice on Ru(0001) and Pt(111), J. Am. Chem. Soc. **138**, 3145 (2016).
[53] N. Gerrard, C. Gattinoni, F. McBride, A. Michaelides, and A. Hodgson, Strain relief during ice growth on a hexagonal template, J. Am. Chem. Soc. **141**, 8599 (2019).